Report

TRANSPARENT PROCESS

EMBO reports

Optogenetic control of mitochondrial protonmotive force to impact cellular stress resistance

Brandon J Berry[1], Adam J Trewin[2], Alexander S Milliken[1], Aksana Baldzizhar[2], Andrea M Amitrano[3,4], Yunki Lim[5], Minsoo Kim[3,4] & Andrew P Wojtovich[1,2,*]

Abstract

Mitochondrial respiration generates an electrochemical proton gradient across the mitochondrial inner membrane called protonmotive force (PMF) to drive diverse functions and synthesize ATP. Current techniques to manipulate the PMF are limited to its dissipation; yet, there is no precise and reversible method to increase the PMF. To address this issue, we aimed to use an optogenetic approach and engineered a mitochondria-targeted light-activated proton pump that we name mitochondria-ON (mtON) to selectively increase the PMF in *Caenorhabditis elegans*. Here we show that mtON photoactivation increases the PMF in a dose-dependent manner, supports ATP synthesis, increases resistance to mitochondrial toxins, and modulates energy-sensing behavior. Moreover, transient mtON activation during hypoxic preconditioning prevents the well-characterized adaptive response of hypoxia resistance. Our results show that optogenetic manipulation of the PMF is a powerful tool to modulate metabolism and cell signaling.

Keywords anoxia; hypoxia; ischemia reperfusion; metabolism; uncoupling
Subject Categories Membranes & Trafficking; Metabolism
DOI 10.15252/embr.201949113 | Received 20 August 2019 | Revised 26 November 2019 | Accepted 15 January 2020 | Published online 11 February 2020
EMBO Reports (2020) 21: e49113

Introduction

Mitochondria generate an electrochemical proton gradient known as the protonmotive force (PMF). This consists of an electrical charge gradient, or membrane potential ($\Delta\psi_m$), and a pH gradient (ΔpH) that drives energy availability and controls diverse physiologic outputs [1–3]. The PMF is generated by proton pumping respiratory complexes of the electron transport chain (ETC) located in the mitochondrial inner membrane (IM). ETC dysfunction can lead to loss of PMF and a diverse range of pathologies [4,5]. For example, because the ETC consumes O_2 to establish the PMF, the PMF is decreased under pathologic hypoxic conditions. The mechanistic link between acute changes in the PMF and downstream physiologic changes is poorly understood [6,7], and research is focused on developing new techniques to elucidate these pathways [8,9].

Stroke is a common pathology in which cells undergo hypoxia and rapid reoxygenation that causes changes in the PMF and compromises mitochondrial functions. Changes in the PMF during hypoxia and reoxygenation influence cell-survival outcomes via mechanisms that are not fully understood [10–13]. Selectively increasing the PMF to distinguish cause and effect in hypoxic models is necessary to open new avenues of investigation that may reveal important metabolic changes that occur in stroke.

There are several techniques that allow experimental modulation of the PMF, but most are pharmacologic and therefore irreversible and not cell- or tissue-specific. Herein, we take a novel approach to overcome these barriers to precisely control the PMF by using optogenetics, adapting an approach used recently to dissipate the PMF [14,15]. One family of widely used optogenetic proteins are bacteriorhodopsin-related light-activated proton pumps. These proteins pump protons across membranes in response to specific wavelengths of light and are often used to study physiology by modulating electrochemical gradients at the plasma membrane [16–18]. Only recently have precise optogenetic techniques been applied to compartmentalized cellular events using light-activated proteins targeted to organelles [14,19,20, preprint: 21,22,23]. Rather than using a non-specific cation channel to permeabilize the IM and dissipate the PMF, here we target the light-activated proton pump from the fungal organism *Leptosphaeria maculans* [16,24] to mitochondria and selectively increase the PMF. We call this optogenetic tool mitochondria-ON (mtON) due to its ability to mimic the proton pumping activity of the ETC in response to light, independent of oxygen or substrate availability.

We validated mtON using the well-characterized genetic model organism, *C. elegans* [4,25,26]. Using hypoxia and reoxygenation, we tested the hypothesis that hypoxia adaptation through preconditioning requires a decreased PMF. Our data demonstrate that transient loss of PMF during preconditioning is necessary and sufficient for resistance to hypoxia. By probing the evolutionarily conserved hypoxia adaptation response [27–30], we show that tools like mtON

1 Department of Pharmacology and Physiology, University of Rochester Medical Center, Rochester, NY, USA
2 Department of Anesthesiology and Perioperative Medicine, University of Rochester Medical Center, Rochester, NY, USA
3 Department of Pathology, University of Rochester Medical Center, Rochester, NY, USA
4 Department of Microbiology and Immunology, University of Rochester Medical Center, Rochester, NY, USA
5 Nephrology Division, Department of Medicine, School of Medicine and Dentistry, University of Rochester Medical Center, Rochester, NY, USA
*Corresponding author. Tel: +1 585 275 4613; E-mail: andrew_wojtovich@urmc.rochester.edu

allow precise determination of cause and effect in physiologic models.

Results and Discussion

Light-activated proton pump mitochondria-ON (mtON) is expressed in mitochondria

Using a ubiquitously expressed gene promoter (P*eft-3*), we directed expression of a light-activated proton pump to the mitochondrial IM in *C. elegans*. Mitochondrial localization was achieved by fusion of the proton pump to an N-terminal mitochondrial targeting sequence of the IMMT1 protein [31,32] in an orientation that allows proton pumping from the mitochondrial matrix toward the intermembrane space to increase the PMF in response to light (Fig 1A). Using a C-terminal mtON::GFP fusion for subcellular visualization, we observed overlap of green and red fluorescence in *C. elegans* tissues stained with MitoTracker™ CMXRos, indicating the intended mitochondrial targeting (Fig 1B). We confirmed the expression of mtON in isolated mitochondrial preparations by immunoblot against GFP and observed a band at the predicted molecular weight of 82 kDa (Fig 1C). To further validate inner mitochondrial membrane targeting, we coexpressed an intermembrane space-targeted mCherry construct with mtON::GFP and measured red and green fluorescence intensities to show expression in different mitochondrial compartments (Fig EV1A–E). In addition, we show that mtON is protected from proteinase K cleavage in swollen, isolated mitochondria (mitoplasts), indicating inner membrane localization and GFP localization in the mitochondrial matrix (Fig EV1F).

mtON activation increases the PMF

Proton pumping activity of mtON requires the cofactor all trans-retinal (ATR) [24,33,34]. Because *C. elegans* do not produce ATR endogenously, exogenous supplementation is required for the light-activated proton pump to function [18,35]. Thus, we were able to control for the expression of mtON (and the included GFP) in functional and non-functional forms, depending on whether ATR was supplemented, in addition to the use of light controls (Fig EV2A–D).

To test whether mtON could generate a PMF, we measured the $\Delta\psi_m$ component using the indicator tetramethylrhodamine ethyl ester (TMRE) in isolated *C. elegans* mitochondria. TMRE is a fluorescent lipophilic cation that will accumulate in mitochondria proportionally with the $\Delta\psi_m$. At the quenching concentration of TMRE used, fluorescence is low at the $\Delta\psi_m$ of intact, energized isolated mitochondria. Upon loss of the $\Delta\psi_m$, TMRE redistributes to the extramitochondrial space resulting in increased fluorescence due to dequenching of TMRE (Fig 2A). Under non-phosphorylating conditions with the ETC inhibited with rotenone and in the absence of added substrate to fuel ETC activity, mtON activation was able to polarize the $\Delta\psi_m$ as much as ETC-driven respiration (Fig 2B) light dose-dependently (Fig EV3A). These data show that more photons result in increased polarization of the PMF, which is in line with the biophysical studies of the proton pump [16]. These data are also in line with the reported proton specificity of the proton pump [16,24]. Light activation of the non-functional pump (no ATR) had no effect on $\Delta\psi_m$ (Fig 2B).

When protons are pumped out of mitochondria during respiration, the matrix pH increases [36]. Thus, we measured pH changes in the mitochondrial matrix in response to light to test this parameter as another readout of mtON activity. Using a ratiometric pH indicator, BCECF-AM, we found that matrix pH increased in response to mtON activation, mimicking the effect of succinate-driven respiration (Fig 2C and D). mtON-stimulated changes in matrix pH and $\Delta\psi_m$ were sensitive to the protonophore FCCP, demonstrating that mtON polarizes the PMF, as measured by both the $\Delta\psi_m$ and the ΔpH, again confirming proton specificity.

mtON increases ATP synthesis without respiration

To further test whether mtON could increase energetics, we measured ATP levels from isolated mitochondria that were supplied with ADP to phosphorylate, since ATP levels are highly regulated *in vivo* [37–40]. As expected, mtON activation increased ATP levels (Fig 2E) light dose-dependently (Fig EV3B), similar to the $\Delta\psi_m$ results. In mitochondria, the amount of ADP converted to ATP is

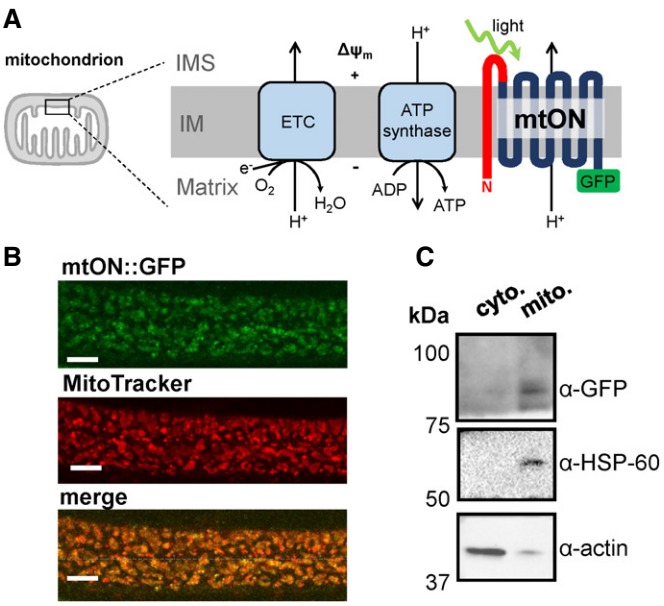

Figure 1. Light-activated proton pump mitochondria-ON (mtON) is expressed in mitochondria.

A Schematic depicting the targeting strategy to localize mtON to the mitochondrial inner membrane (IM). The electron transport chain (ETC) complexes generate the endogenous mitochondrial PMF by proton pumping, represented by the + and − across the IM. Mitochondrial ATP synthase utilizes the PMF to convert ADP to ATP. The N-terminal mitochondria-target sequence from the IMMT1 protein shown in red; GFP shown in green. In response to light, mtON pumps protons from the mitochondrial matrix to the intermembrane space (IMS).

B Confocal images demonstrate overlap of GFP-tagged mtON with MitoTracker™ Red CMXRos-stained *Caenorhabditis elegans* hypodermal mitochondria. Scale bar 10 μm.

C Immunoblot comparing the cytosolic supernatant and the mitochondria-enriched pellet of isolation fractions. GFP-tagged mtON migrates at the predicted molecular weight of 82 kDa accounting for the mitochondria-target sequence, the proton pump, and GFP. mtON is observed only in the mitochondrial fraction compared to marker proteins HSP60 (mitochondria) and actin (cytosol). All blots are from the same lanes on one membrane.

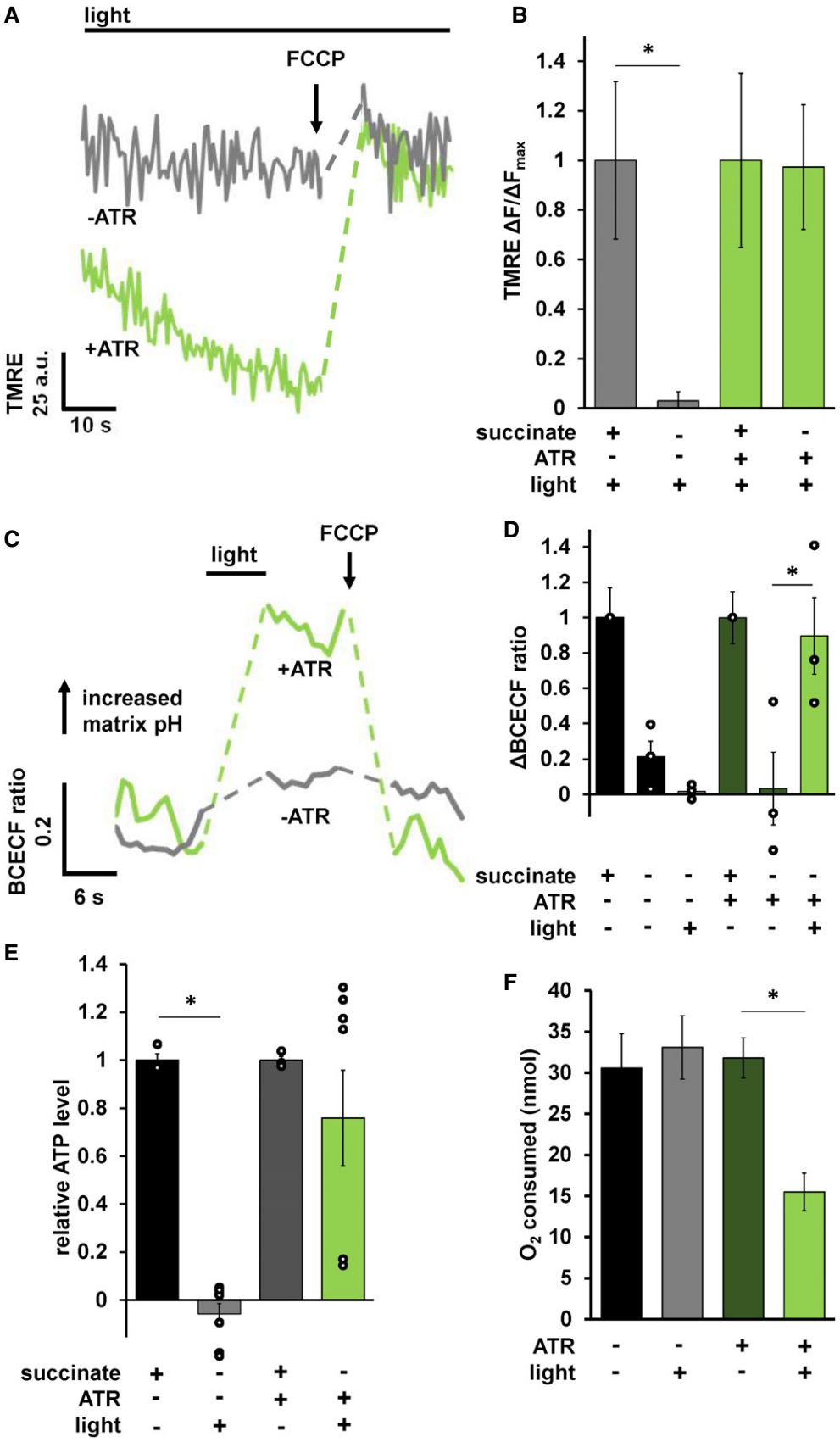
A
light
FCCP
-ATR
+ATR
TMRE
25 a.u.
10 s
B
TMRE ΔF/ΔF max
succinate + - + -
ATR - - + +
light + + + +
C
light
FCCP
+ATR
increased
matrix pH
-ATR
BCECF ratio
0.2
6 s
D
ΔBCECF ratio
succinate + - - + - -
ATR - - - + + +
light - - + - - +
E
relative ATP level
succinate + - + -
ATR - - + +
light - + - +
F
O2 consumed (nmol)
ATR - - + +
light - + - +

Figure 2.

Figure 2. mtON activation increases the PMF.

A Representative TMRE fluorescence traces in arbitrary units (a.u.) before and after $\Delta\psi_m$ dissipation with FCCP. Dashed lines indicate where FCCP was added. +/− ATR traces were performed in the absence of succinate. mtON activation was continuous throughout the traces. Light green trace is from mitochondria with ATR, gray traces are without.

B Quantification of change in fluorescence (ΔF) normalized to the maximum change in fluorescence given by succinate respiration (ΔF_{max}) for each mitochondrial preparation. Data are from the maximum light dose in Fig EV3A. Two-way ANOVA with Sidak's test for multiple comparisons, *P = 0.0469, +ATR succinate versus +ATR +light P = 0.9978, n = 6 mitochondrial isolations. Data show mean ± SEM.

C Representative BCECF-AM 490/440 nm ratio trace. Ratio of 545 nm fluorescence intensity at either 440 or 490 nm excitation. Dashed lines are where light or FCCP treatment occurred. Light green trace is from mitochondria with ATR, gray traces are without.

D Quantification of change in BCECF-AM fluorescence ratio normalized to maximum change given by succinate matrix alkalization. Two-way ANOVA with Sidak's test for multiple comparisons, −ATR succinate versus −ATR, +light *P = 0.0212, +ATR succinate versus +ATR light P = 0.999, +ATR succinate versus +ATR, −light P = 0.0237, +ATR, +light versus, +ATR, −light P = 0.0474, n = 3 mitochondrial isolations. Some individual points overlap. Data show mean ± SEM.

E ATP levels normalized to total ATP synthesis given by succinate respiration. Data from Fig EV3B. Succinate data shown for comparison after normalization. Two-way ANOVA with Sidak's test for multiple comparisons, *P = 0.0011, +ATR succinate versus +ATR light P = 0.5680, n = 3, 7, 3, 7 biological replicates for each bar from left to right. Some individual points overlap. Data show mean ± SEM.

F O_2 required to consume 50 nmoles of ADP after mtON activation. Data are the maximum illumination from Fig EV4D using time-matched dark conditions, one-way ANOVA *P = 0.013 (−ATR, −light versus +ATR, +light P = 0.010. −ATR, +light versus +ATR, +light P = 0.013.) −ATR, −light n = 5, rest n = 6 mitochondrial preparations. Data show mean ± SEM.

reliant on O_2 consumption by the ETC [41]. We tested whether we could drive ADP conversion to ATP by generating a PMF with mtON, bypassing the requirement for O_2 consumption. Respiration was consistent across all control conditions (Fig EV4A and B), indicating no baseline differences in mitochondrial quality. Activation of mtON decreased the amount of O_2 required to phosphorylate a given amount of ADP (Figs 2F and EV4C) light dose-dependently (Fig EV4D), indicating mtON-driven ATP production does not rely on O_2 consumption. Until now, interventions to increase the PMF have involved fueling the ETC, where here we show mtON generates a PMF independent of O_2 consumption or metabolic substrates to provide electrons. mtON's ability to augment the PMF via optic control opens a new avenue for discovery in metabolic research where complex interactions between physiology and bioenergetics often obscure molecular mechanisms.

mtON reverses and controls mitochondrial dysfunction

Given that mtON activity decreased reliance on the ETC *in vitro*, we tested whether mtON could compensate for acute ETC dysfunction *in vivo*. We exposed *C. elegans* to toxic inhibitors of specific sites within ETC complexes and scored their survival in response to mtON activation. Light alone had no effect on survival after inhibitor exposure in all cases (Fig 3A–D). For transgenic animals, when exposed to the complex I inhibitor rotenone, mtON was able to improve survival (Fig 3A). Rotenone toxicity is mediated chiefly through oxidative damage [42,43], and ATR alone exhibited a protective effect under these conditions, possibly due to its antioxidant properties [44–46]. This effect was also present in wild-type control experiments (Fig EV5A). However, the effect of mtON was significantly greater than the ATR effect (Fig EV5A, one-way ANOVA, P = 0.0002), with no effect in wild-type animals (Fig EV5A and B). Activation of mtON also protected animals exposed to antimycin A, a complex III inhibitor [42] (Fig 3B), and azide, a complex IV inhibitor (Fig 3C). Unlike with rotenone treatment, ATR alone did not mitigate antimycin A or azide toxicity. mtON-expressing animals could not overcome toxicity mediated by the ATP synthase inhibitor, oligomycin A (Fig 3D). Overall, these data indicate that mtON can partially overcome inhibited ETC activity in whole organisms, but not direct inhibition of ATP synthesis downstream of the PMF, as expected. These observations are supported in part by previous *in vitro* evidence from cells with mitochondria expressing a mitochondria-targeted rhodopsin [23].

To further test whether mtON could compensate for a dysfunctional ETC, we expressed it in a complex I mutant background (*gas-1*). *gas-1* animals have a decreased locomotion (Fig 3E), various impaired behaviors [47,48], and decreased mitochondrial membrane potential [4]. mtON activation was able to partially rescue locomotion in the *gas-1* mutant background, suggesting the impaired locomotion is due to the reported decreased PMF.

To characterize a more adaptive response in a mitochondrial mutant background, we chose a strain of animals harboring a mitochondrial DNA (mtDNA) deletion, the uaDf5 deletion [49]. Animals with uaDf5 mtDNA have upregulated compensatory mechanisms to promote survival [50], as do many mitochondrial mutants [51,52]. Importantly, maintenance of the uaDf5 mtDNA relies on the mitochondrial unfolded protein response, a stress resistance program that requires the PMF [53], as do many mitochondrial quality control pathways. Therefore, we reasoned that mtON activation in the uaDf5 harboring strain would artificially signal healthy mitochondria and suppress adaptive signaling. We expressed mtON in the uaDf5 mutant background and confirmed mtDNA heteroplasmy (Fig EV5C). We found that mtON activation in adult animals resulted in synthetic lethality (Fig EV5D). This result is in line with our prediction that increasing the PMF suppresses adaptive signaling mediated by damaged or PMF-compromised mitochondria. This result also shows the importance of temporal control when studying effects of the PMF, where different outcomes are possible when observing chronic versus acute changes in mitochondrial function. In other words, increasing the PMF at different times or for different durations can be either beneficial or detrimental, depending on the context.

While this work was under revision, a similar technique using an alternative light-activated proton pump was characterized in a *Drosophila* model [54], supporting our findings and demonstrating the broad application of these optogenetic tools in neurodegeneration. Our results with mtON compliment these findings and expand them in other areas including the following energy sensing and hypoxia adaptation studies.

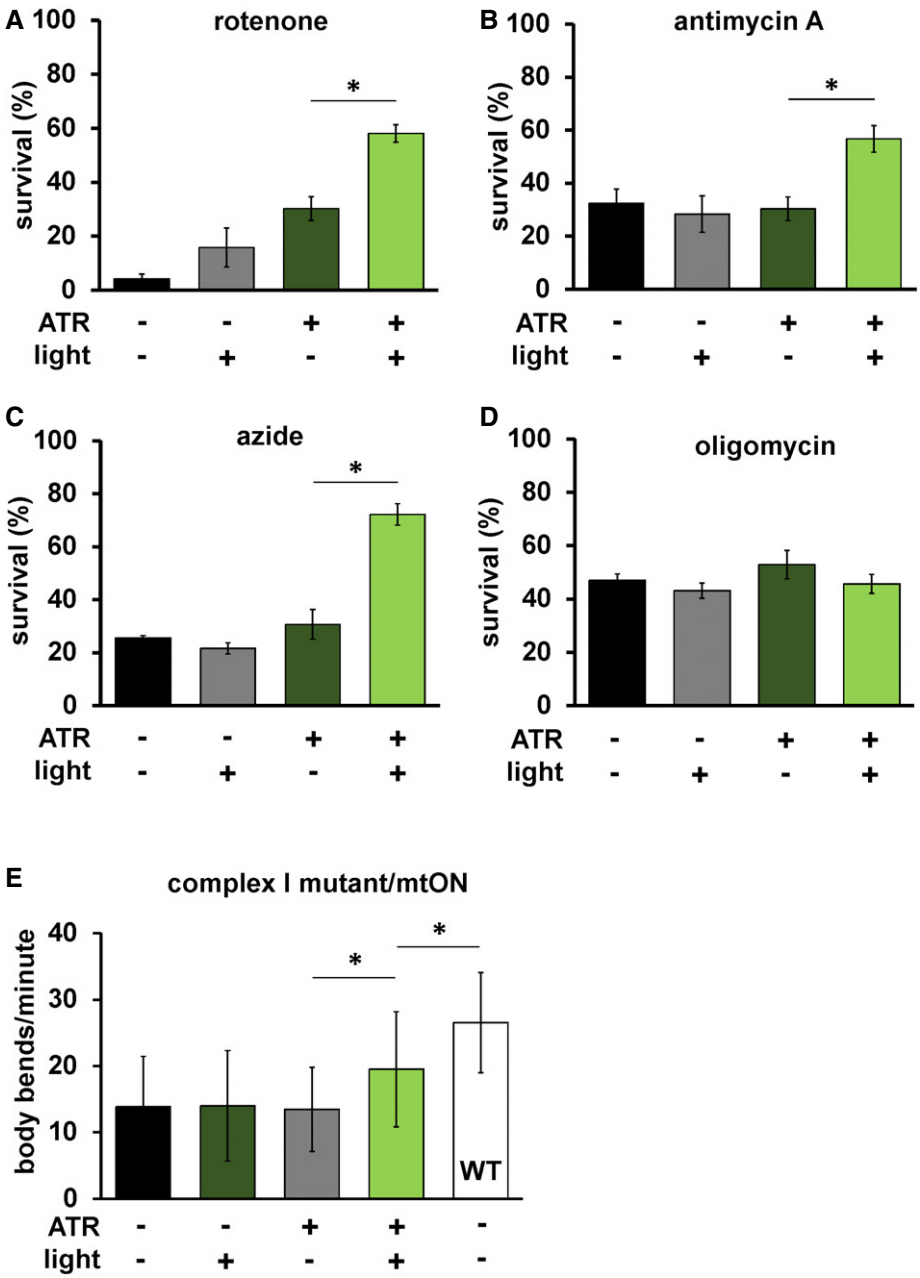

Figure 3. mtON reverses mitochondrial dysfunction.

A Day 1 adult animals expressing mtON were exposed to 50 μM rotenone (ETC complex I inhibitor) for 5 h, and survival was scored. Illumination was continuous throughout toxin exposure (see Materials and Methods). ATR alone was protective (−ATR, −light versus +ATR, −light $P = 0.016$.) The effect of mtON activation was greater than the ATR alone effect, one-way ANOVA with Tukey's post hoc test $^*P = 0.01$. (−ATR, −light versus +ATR, +light $P = 0.0002$. −ATR, +light versus +ATR, +light $P = 0.0009$. $n = 3$ plates each condition with at least 15 animals per plate). Data show mean ± SEM.

B mtON-expressing animals were exposed to 50 μM antimycin A (complex III inhibitor), and survival was scored 18 h later. One-way ANOVA with Tukey's post hoc test $^*P = 0.02$ (−ATR, −light versus +ATR, +light $P = 0.03$, −ATR, +light versus +ATR, +light $P = 0.01$. $n = 5$ plates each condition with at least 15 animals per plate). Data show mean ± SEM.

C mtON-expressing animals were exposed to 0.25 M azide (complex IV inhibitor) for 1 h and scored for survival 1 h after recovering, one-way ANOVA with Tukey's post hoc test $^*P = 0.0002$. (−ATR, −light versus +ATR, +light $P < 0.0001$, −ATR, +light versus +ATR, +light $P < 0.0001$. $n = 3$ plates each condition with at least 15 animals per plate). Data show mean ± SEM.

D mtON-expressing animals were exposed to 31 μM oligomycin A (ATP synthase inhibitor), and survival was scored 18 h later. No significant differences were found by one-way ANOVA ($n = 3$ plates each condition with at least 15 animals per plate). Data show mean ± SEM.

E mtON-expressing animals in a complex I mutant background (*gas-1)* were scored for locomotion speed in the presence of food by counting body bends per minute. mtON activation rescued the decreased locomotion of the *gas-1* mutant background, one-way ANOVA with Tukey's post hoc test, −ATR, +light versus +ATR, +light $^*P = 0.0145$, +ATR, +light versus wild type (WT) $^*P = 0.0008$ (−ATR, −light versus +ATR, +light $P = 0.0272$, +ATR, −light versus +ATR, +light $P = 0.0332$, all conditions versus WT, $P < 0.001$, $n = 30, 30, 30, 41, 41$ animals each bar from left to right). Data show mean ± standard deviation.

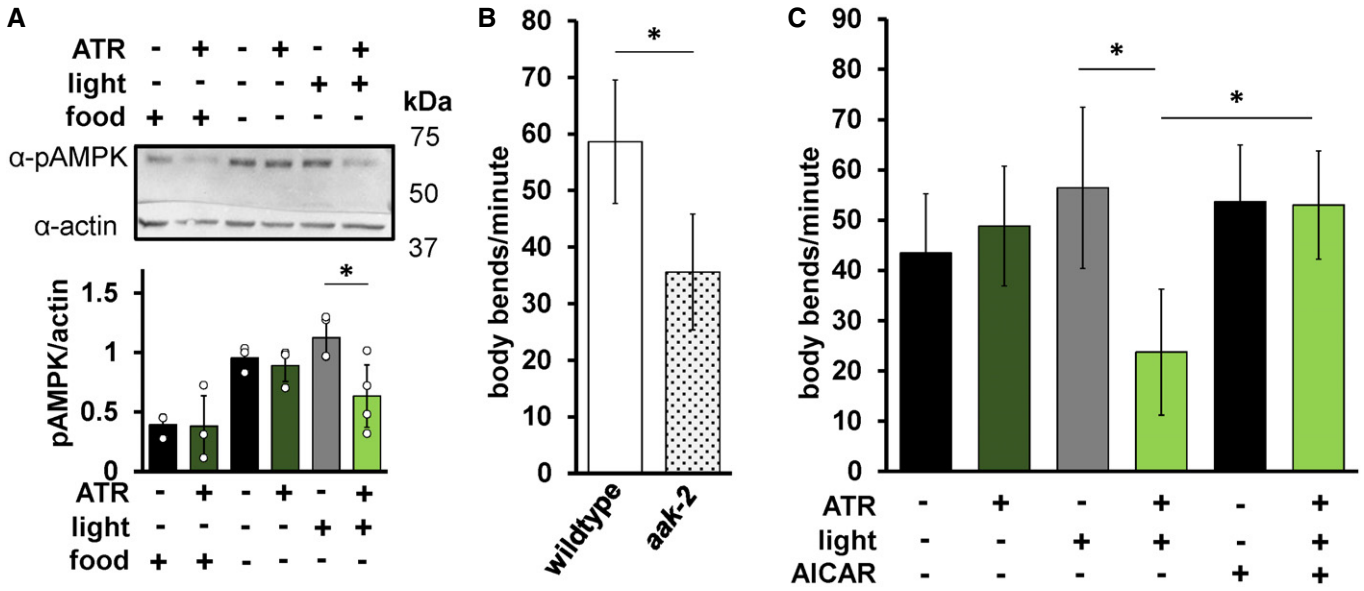

Figure 4. mtON affects whole-animal energy sensing.

A Top: immunoblot assessing the effect of mtON activation on AMPK phosphorylation status. Top bands (~62 kDa) are phosphorylated AMPK signal, and bottom bands (~43 kDa) are actin signal. Image is from the same membrane cut to separately probe for phosphorylated AMPK (pAMPK) and actin. Bottom: densitometry analysis showing decreased pAMPK to actin ratio, as there is no known antibody directed against total AMPK in *Caenorhabditis elegans.* Phosphorylation increases in the absence of food, but low phosphorylation is preserved when mtON is activated, two-way ANOVA with Sidak's test for multiple comparisons, $*P = 0.0203$, $n = 3, 3, 3, 4, 4$ biological replicates each bar from left to right. Data show mean ± standard deviation.

B Locomotion was assessed by counting body bends per minute. Wild-type animals were compared to *aak-2(ok524)* mutant animals. Two-sample, 2-tailed unpaired *t*-test $*P < 0.0001$, wild-type $n = 35$, *aak-2* $n = 39$ animals across at least 3 days. Data show mean ± standard deviation.

C Locomotion in response to mtON activation. Illumination was continuous throughout body bends measurement (see Materials and Methods). For AAK-2 activation, animals were exposed to 1 mM AICAR for 4 h before body bend measurement. One-way ANOVA with Tukey's post hoc test, −ATR, +light versus +ATR, +light $*P < 0.0001$, +ATR, +light versus AICAR $*P < 0.0001$, +ATR, +light versus AICAR +light $*P < 0.0001$. $n = 36, 39, 37, 46, 36, 36$ animals each bar from left to right. Data show mean ± standard deviation.

mtON affects whole-animal energy sensing

We next asked whether mtON could affect metabolic signaling. One way organisms sense energy availability and preserve energy homeostasis is through AMP-activated protein kinase (AMPK) signaling [55]. In *C. elegans,* the *aak-2* gene encodes the catalytic subunit ortholog of mammalian AMPKα2. Mutation of *aak-2* has well-characterized phenotypic outputs linked to energy availability and serves as a regulator of whole-organism energy sensing [56,57]. We hypothesized that mtON activity would signal energy availability and decrease phosphorylation of AMPK, its activated state. As such, we exposed animals expressing mtON to light in the absence of food, where AMPK should be phosphorylated, and immunoblotted against phosphorylated AMPK. We found that removal from food increases AMPK phosphorylation as expected, and mtON activation prevented this phosphorylation (Fig 4A). In *C. elegans,* the AMPK homologue AAK-2 regulates a behavioral response to food availability [58], where in the absence of food animals will increase locomotion to search for food. Based on our phosphorylation results, we

Figure 5. mtON inhibits hypoxia adaptation.

A Schematic of HR experiments. Top shows control hypoxia and reoxygenation. Below is the hypoxic preconditioning (PC) protocol, survival for these two timelines shown in panel B. Third from the top shows FCCP treatment protocol, calculated protection shown in panel C. Fourth and fifth from the top show light treatment protocol + and − PC, calculated protection data from these protocols shown in panel D. Bottom shows light treatment during hypoxia, calculated protection data from these protocols shown in panel E.

B Survival after HR in day 1 adult animals is shown with hypoxic preconditioning (PC, represented by diagonal stripes) 2-sample 2-tailed unpaired *t*-test, ctrl versus PC $*P = 0.0035$, $n = 4$, each averaged from 3 technical replicates with at least 15 animals per replicate. Data show mean ± SEM.

C Protection (%) is percent survival minus percent survival of control condition. PC data calculated from panel B. FCCP final concentrations 0.001, 0.01, 0.1, 1 nM. One-way ANOVA with Tukey's post hoc test, PC versus 0.001 nM FCCP, $*P = 0.0012$, 0.001 nM FCCP versus 0.01 FCCP, $*P = 0.0142$, $n = 4, 3, 3, 3, 3$ independent experiments each bar from left to right, each averaged from 3 technical replicates with at least 15 animals per replicate. Data show mean ± SEM.

D Illumination was continuous throughout PC alone; control illumination was for the same duration under normoxic conditions (see Materials and Methods, panel A). Two-way ANOVA comparing +ATR versus −ATR in each group. $*P = 0.016$, $n = 11, 11, 4, 4, 6, 6$ independent experiments each bar from left to right, each averaged from 3 technical replicates with at least 15 animals per replicate. Data show mean ± SEM.

E Light during hypoxia. Two-sample 2-tailed unpaired *t*-test, $*P = 0.0276$, $n = 7$ independent experiments, each averaged from 3 technical replicates with at least 15 animals per replicate. Data show mean ± SEM.

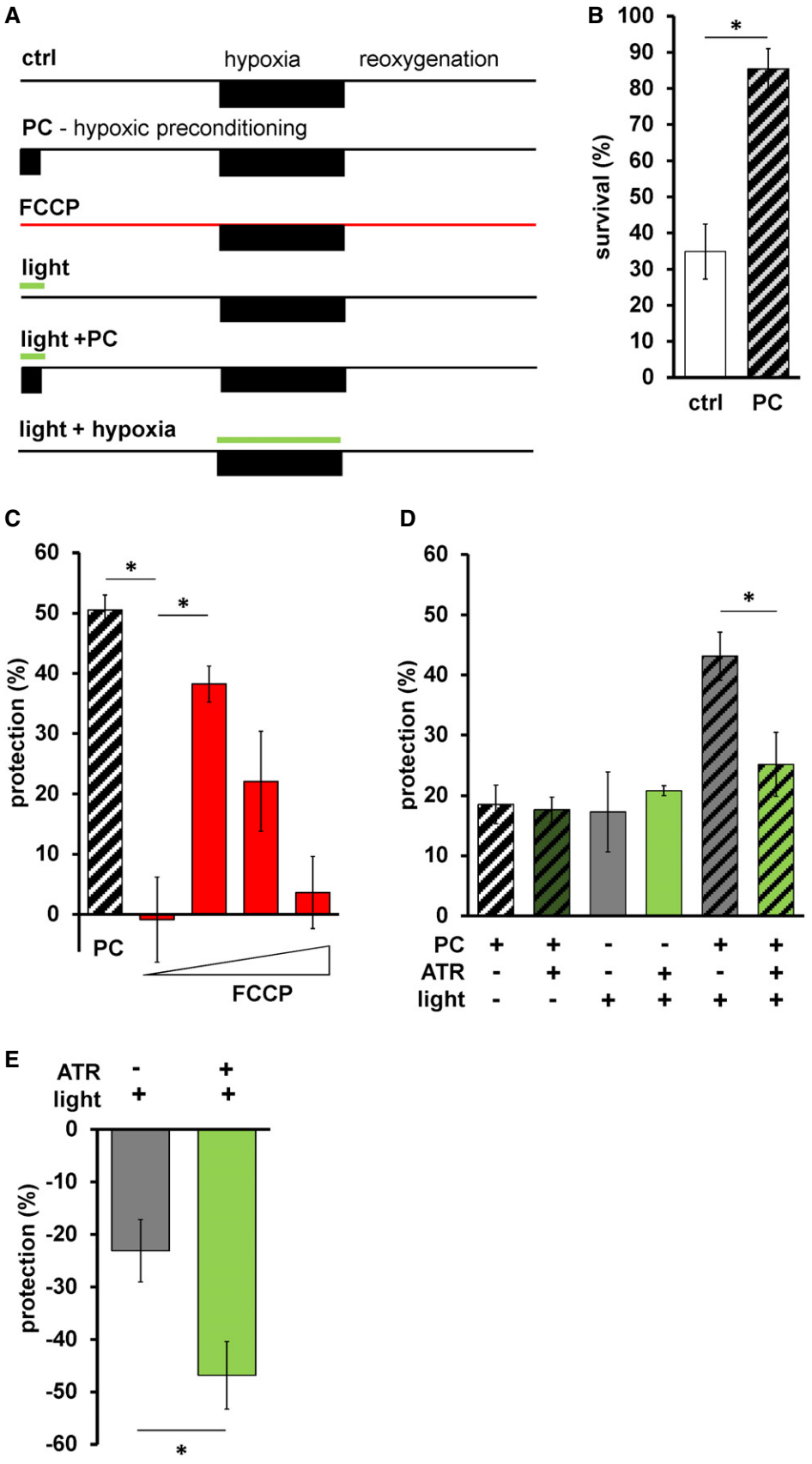
A
ctrl
hypoxia
reoxygenation
PC - hypoxic preconditioning
FCCP
light
light +PC
light + hypoxia
B
survival (%)
ctrl
PC
C
protection (%)
PC
FCCP
D
protection (%)
PC
ATR
light
E
ATR
light
protection (%)

Figure 5.

hypothesized that mtON activation would attenuate the energy deficit signal for animals off food, suppressing their movement and thus mimicking the *aak-2* loss-of-function phenotype. We first confirmed that *aak-2* loss-of-function mutant animals had decreased locomotion in the absence of food compared to wild type (Fig 4B). In response to acute mtON activation in wild-type background, we observed decreased locomotion in the absence of food (Fig 4C). This effect was reversed using the AMPK activator 5-aminoimidazole-4-carboxamide ribonucleotide (AICAR), indicating the mtON suppression of locomotion was rescued by AMPK activity (Fig 4C). These data suggest that mtON activity can modify downstream metabolic signaling. As changing the PMF affects many aspects of metabolism that can activate AMPK, the exact mechanism of AMPK activation in our experiments is unclear. For example, AMPK is activated by increased energy demand, but also redox signaling [59] and calcium signaling [60]. Upon further characterization in these contexts, mtON could be used to modulate the many cellular processes that AMPK regulates [61–64].

mtON inhibits hypoxia adaptation

We next tested whether mtON could impact hypoxic stress resistance. Hypoxia and reoxygenation (HR) is a pathologic insult that involves changes in the PMF that can contribute to injury and survival [11–13,65–68] depending on the context and degree of (de)polarization. In addition, the phenomenon of preconditioning (PC) is effectively modeled with hypoxia in *C. elegans* [28,69–72], where a short period of hypoxia protects against a later pathologic exposure (Fig 5B). A decreased PMF before HR also mediates a protective effect [73–75], but mechanisms are debated [76], as understanding is complicated by lack of temporal control when using pharmacologic approaches. In support of this, the protonophore FCCP, which can dissipate the PMF, protected wild-type animals against HR (Fig 5C), suggesting hypoxia resistance may be mediated by a decreased PMF. We combined these lines of evidence and hypothesized that increasing the PMF during PC would reverse the protection against hypoxia afforded by PC. To test this hypothesis, we activated mtON selectively during PC (Fig 5A). To quantify protection, we subtracted the percent survival after pathologic hypoxia from the percent survival after an intervention, giving the percent alive above baseline (Fig 5C). Further highlighting the importance of our control conditions, we found that light on its own was as protective as PC in mtON-expressing animals, and the combination of light and PC was additive (Fig 5D). However, activation of mtON during PC decreased the protection (Fig 5D), supporting our hypothesis that some of the protective effect of PC is mediated by decreasing the PMF. In effect, mtON counteracts a PC-induced decrease in the PMF by restoring it to normal levels. These data suggest that loss of PMF during PC is necessary for hypoxic adaptation, and should be further investigated in the context of redox changes that may contribute to the light-alone result. The FCCP data corroborate our mtON findings, however, and demonstrate the sufficiency of PMF loss to protect against hypoxia. Using mtON only during PC to boost the PMF provided temporal control that had not been tested before, allowing us to determine when PMF changes have physiologic effects in HR.

Then, we tested the effect of mtON activation during pathologic hypoxia and found that mtON mediated a damaging effect (Fig 5E), above the damaging effect of light on its own [77]. Maintaining the PMF throughout hypoxia with mtON may drive damage at reoxygenation by increasing mitochondrial cation accumulation and damaging ROS resulting from the increased PMF at reoxygenation [66]. Further, *C. elegans* enter a suspended animation state under hypoxia [78] that may contribute to hypoxic survival [79], and this state may have been reversed by mtON activation. This result provides more evidence that temporal control of the PMF alters different aspects of hypoxic pathology time-dependently, where during preconditioning loss of PMF signals protection, and during hypoxia increased PMF drives pathology.

Our findings that protection afforded by PC relies on the transient loss of PMF suggest that a decreased PMF is sufficient to elicit stress resistance at a later period. This implies that interventions at the level of the PMF alone can impact cellular responses to stress. Combining the mtON approach with tissue-specific gene promoters, precise spatiotemporal control could be achieved in discerning the effects of mitochondrial function across tissues in whole organisms. Taken together, mtON appears to be a useful tool to enable discrimination of cause and effect in complex (patho)physiologic contexts that involve modest changes in mitochondrial function and metabolism. Defining when changes in the PMF are adaptive and when they are detrimental may advance our understanding of many pathologies and inform novel therapeutic strategies that target mitochondrial function. Our findings from this approach suggest the PMF is a keystone of metabolism that senses cellular stress and elicits appropriate adaptive responses to maintain homeostasis.

Materials and Methods

Molecular biology

The light-activated proton pump from *Leptosphaeria maculans* (Mac) fused to eGFP was amplified from plasmid DNA pFCK-Mac-GFP, a gift from Edward Boyden (Addgene plasmid #22223 [16]) (forward amplification primer: ACACCTGCAGGCTTGATCGTGGAC CAGTTCGA, reverse amplification primer: CACAGCGGCCGCTTACT TGTACAGCTCGTCCA). The N-terminal 187 amino acids of the *Immt1* gene were amplified by PCR from mouse cDNA (forward amplification primer: ACAACCGGTAAAAATGCTGCGGGCCTGTCA GTT, reverse amplification primer: CACCCTGCAGGTTCCTCTGTGG TTTCAGACG). The ubiquitously expressed gene promoter P*eft-3* (also known as P*eef-1A.1*) was amplified by PCR from pDD162 (forward amplification primer: AACAAAGCTTGCACCTTTGGTCTTTTA, reverse amplification primer: ACATCTAGAGAGCAAAGTGTTTCC CA). The body wall muscle promoter P*myo-3* was PCR amplified from pDJ16 (forward amplification primer: ACAGCTAGCTGTGTGT GATTGCT, reverse amplification primer: ACAACCGGTGCGGCAATT CTAGATGG). PCR fragments were ligated into pFH6.II (pPD95.81 with a modified multi-cloning site) for *C. elegans* expression using restriction digest cloning. Resulting plasmids were pBJB20 (P*eft-3*::IMMT1(N-terminal 187 amino acids)::Mac::GFP) and pBJB16 (P*myo-3*::IMMT1(N-terminal 187 amino acids)::Mac::GFP), and Sanger sequencing was used to confirm plasmid sequences

(Eurofins Genomics). Animals were transformed by plasmid DNA microinjection with *pha-1(+)* selection in *a pha-1(e2123ts)* temperature-sensitive mutant strain, where transgenic animals were selected for growth at 20°C.

Caenorhabditis elegans strains growth and maintenance

All animals were maintained at 20°C on nematode growth medium (NGM) seeded with OP50 *E. coli.* Young adult hermaphrodite animals were used for all experiments. Transgenic strains were generated by plasmid DNA microinjection as described [80]. For a complete strain list, see Table EV1. Where indicated, OP50 was supplemented with all trans-retinal to a final concentration of 100 μM on seeded NGM plates. Animals were cultured on ATR-containing plates for at least one generation. The strain APW138 was generated by homology-directed genome editing through CRISPR/Cas9 as previously described [81,82]. Briefly, the endogenous IMMT-1 protein was fused with the red fluorescent protein mCherry with a linker region on the C-terminus. mCherry was amplified from plasmid DNA pCFJ90 (forward amplification primer: CTCGCCCAGCTTCTTGTGGCTCACGCCGCC GTCTCATCGATTCGCTCAACTTATCCTCGTAGCCCTCGGACTCCTC GTAGCATGGTCTCAAAGGGTGAAGA, reverse amplification primer: TTTTAAAAAACGGTGACGCAAGACAATCAATTGTTCTAC TTATACAATTCATCCATGCC) and microinjected into *C. elegans* hermaphrodite gonads with purified Cas9 protein and crRNA (CTAATAAGTTGAGCGAATCG, DNA target) to achieve transgene insertion into the genome of progeny. The transgenic line generated by CRISPR/Cas9 was outcrossed four times to the wild-type strain.

Fluorescence microscopy

Images were taken on a FV1000 Olympus laser scanning confocal microscope using a 60× oil objective (Olympus, N.A. 1.42). Diode laser illumination was at 561 nm for red fluorescence and 488 nm for green fluorescence. Where indicated, animals were stained with 10 μM MitoTracker™ Red CMXRos for 4 h. MitoTracker™ stain was dissolved in DMSO, diluted in M9 media (22 mM KH_2PO_4, 42 mM Na_2HPO_4, 86 mM NaCl, 1 mM $MgSO_4$, pH 7), and added to OP50 seeded NGM plates (DMSO < 0.02% final) and allowed to dry. Line scan pixel intensity was performed using ImageJ software. Fluorescent determination of mtON localization was performed as previously reported [22]. Briefly, cross-section intensity plots of muscle mitochondrial fluorescence (coexpressing either mtON::GFP and mCherry, or mtON animals stained with MitoTracker) were smoothed by three-point moving averages and then normalized to maximum intensity of each intensity trace. Distance between maximum red and green signal was calculated, as well as the distance between inflection points (defined as a threshold of 10% increase in pixel intensity from the previous point, in the direction from outer border toward the middle of the mitochondrion).

Mitochondria isolation

Caenorhabditis elegans mitochondria were isolated from day 1 adults as previously described [70] using differential centrifugation in mannitol and sucrose-based media. Animals from three 15-cm culture plates were transferred into 50 ml of M9 media in a conical tube and allowed to settle by gravity on ice. Pelleted animals were rinsed with ice-cold M9 twice and once with ice-cold mitochondrial isolation media (220 mM mannitol, 70 mM sucrose, 5 mM MOPS, 2 mM EGTA, pH 7.4) with 0.04% BSA. After settling by gravity, supernatant was removed and worms were transferred to an ice-cold mortar containing ~2 g of pure sea sand per 1 ml of animals. Animals were ground with an ice-cold pestle for 1 min and extracted from the sand using mitochondrial isolation media and transferred to a 10-ml conical tube. The suspension was then transferred to an ice-cold glass Dounce homogenizer and homogenized with 40 strokes. The homogenate was centrifuged at 600 *g* for 5 min. Supernatant was transferred to a new tube and centrifuged at 700 *g* for 10 min. The pellet was resuspended in 1 ml of mitochondrial isolation media without BSA, which was centrifuged at 7,000 *g* for 5 min. The pellet was finally resuspended in 50 μl of mitochondrial isolation media without BSA. Protein concentration was quantified using the Folin-phenol method.

Light sources

Illumination sources included a 580 nm Quantum SpectraLife LED Hybrid lamp by Quantum Devices, Barneveld WI, USA (abbreviated Quantum LED), a 540–600 nm GYX module, XCite LED1 by Excelitas, Waltham MA, USA (abbreviated XCite LED), and a 540–580 nm excitation filter MVX10 Fluorescence MacroZoom dissecting microscope by Olympus (abbreviated MVX). Light intensities are indicated for each experimental condition and were determined with a calibrated thermopile detector (818P-010-12, Newport Corporation, Irvine, CA) and optical power meter (1916-R, Newport Corporation).

Immunoblotting

Synchronized young adult animals were exposed to 1 Hz light (Quantum LED, 0.02 mW/mm^2) for 4 h, and immediately harvested with ice-cold M9 media and centrifuged at 1,000× *g* for 1 min. Animals were ground by plastic pestle disruption in lysis buffer (20 mM Tris–HCl, 100 mM NaCl, 1 mM EDTA, 1 mM DTT, 10% glycerol, 0.1% SDS, pH 7.6, 1× Halt™ protease inhibitor cocktail, Thermo78429) and diluted 1:1 in sample loading buffer (100 mM Tris–HCl, 10% v/v glycerol, 10% SDS, 0.2% w/v bromophenol blue, 2% v/v β-mercaptoethanol). These samples were heated at 95°C for 5 min. Isolated mitochondrial samples were prepared as described above and diluted 1:1 in sample loading buffer with 1% SDS. 30 μg samples were loaded to 7.5% polyacrylamide gels and separated by SDS–PAGE. Proteins were transferred to nitrocellulose membranes and blocked in 5% non-fat milk/TBST (50 mM Tris, 150 mM NaCl, 0.05% Tween 20, pH 8.0) for 1 h at room temperature. Membranes were incubated at 4°C in primary antibodies diluted 1:1,000 in 5% bovine serum albumin: anti-GFP (ClonTech Living Colours #ab632375), anti-ATP5a (Abcam, #ab14748), 1:60 anti-HSP60 (Department of Biology, Iowa City, IA 52242; Developmental Studies Hybridoma Bank, University of Iowa Department of Biology, Iowa City, IA 52242), (Cell Signaling, #4188), anti-Actin (Abcam #ab14128), and 1:10,000 anti-phospho-AMPKα Rabbit (Cell Signaling, #2535). Membranes were washed in TBST and incubated in horseradish peroxidase-conjugated secondary antibodies: 1:2,000 anti-rabbit IgG (Cell Signaling

#7074S) or anti-mouse IgG (Thermo Scientific #32430, lot #RF234708) for 1 h at room temperature. Proteins were visualized using ECL (Clarity Western ECL Substrate, Bio-Rad) by chemiluminescence (ChemiDoc, Bio-Rad). Densitometry was performed using Image Lab software (version 5.2.1).

Protease protection assay

Inner membrane localization was determined as previously reported [22]. Briefly, mitochondria were isolated as described and pelleted at 7,000 *g* for 5 min, and then, the supernatant was removed. Mitochondria were resuspended in hypotonic swelling buffer (20 mM HEPES, 1 mM EGTA, pH 7.2 at 4°C) and incubated on ice for 10 min. Mitochondria were then pelleted again at 7,000 *g* for 5 min and then resuspended in MRB. Samples were treated with proteinase K (No. P81075; Biolabs) at 0.08 U/mg protein^{-1} for 10 min with or without Triton X (2.5% v/v), and then, digestion was inhibited with the serine protease inhibitor, phenylmethylsulfonyl fluoride (PMSF, 40 mM). Sample loading buffer was added 1:1, and the SDS-denatured protein lysates were resolved on a 7.5% polyacrylamide gel as described above.

Mitochondrial membrane potential measurement

Isolated mitochondria at 0.5 mg/ml were stirred in mitochondrial respiration buffer (MRB: 120 mM KCl, 25 mM sucrose, 5 mM $MgCl_2$, 5 mM KH_2PO_4, 1 mM EGTA, 10 mM HEPES, 1 mg/ml FF-BSA, pH 7.35) at 25°C in the presence of 2 μM rotenone and 5 mM succinate where indicated. 300 nM tetramethylrhodamine ethyl ester (TMRE, Thermo Fisher, T669) was added to observe mitochondrial membrane potential in quench mode. Under quenching conditions, TMRE fluorescence is low in the presence of a $\Delta\psi_m$. Upon addition of a protonophore (e.g., FCCP), TMRE will exit mitochondria and dequench and increase total fluorescence [66,83]. TMRE signal was measured by Cary Eclipse Fluorescence Spectrophotometer (Agilent Technologies) using a 335–620 nm excitation filter and a 550–1,100 nm emission. Illumination was performed continuously throughout all measurements (555 nm, 0.0016 mW/mm^2). Increasing illumination time exposed mitochondria to more photons (calculated as fluence, J/cm^2). After stable baseline measurements with or without succinate, 2 μM FCCP was added to completely depolarize mitochondria. The average fluorescence intensity after addition of 2 μM FCCP (maximum fluorescence in quench mode) was subtracted from the starting test condition to give a change in fluorescence corresponding to changes in $\Delta\psi_m$ (ΔF for conditions without succinate, and ΔF_{max} for conditions with succinate). To represent polarization of the $\Delta\psi_m$, we used the ratio of change in fluorescence (ΔF, FCCP fluorescence minus experimental fluorescence) to the maximum change in fluorescence generated by succinate-driven $\Delta\psi_m$ (ΔF_{max}).

Mitochondrial matrix pH measurement

The ratiometric pH indicator BCECF-AM (Thermo Fisher, B1170) was used to measure pH changes in the mitochondrial matrix [84] in response to succinate respiration or mtON activation. Isolated mitochondria (~200 μl per isolation) were incubated at room temperature with 50 μM BCECF-AM for 10 min with periodic mixing. Mitochondria were then pelleted at 7,000 *g* for 5 min at 4°C, and isolation media replaced and pelleted again to remove extramitochondrial BCECF-AM. Isolated mitochondrial suspensions were then assayed under the same conditions as in the mitochondrial membrane potential measurements described above. Ratiometric fluorescent signal was measured by Cary Eclipse Fluorescence Spectrophotometer (Agilent Technologies) using 440 and 490 nm excitation wavelengths and 545 nm emission. The fluorescence intensity ratio at 545 nm of 490/440 nm excitation wavelengths was used to represent pH changes in the mitochondrial matrix. Light treatment was 0.16 J/cm^2 (XCite LED, 0.02 mW/mm^2), and 2 μM FCCP was used at the end of each trace to establish baseline signal.

ATP measurement

Relative ATP levels were determined in isolated mitochondria given a known amount of ADP to test the ability of mtON to drive ATP synthesis. We used a luciferase bioluminescence kit according to the manufacturer's instructions (Invitrogen™ Molecular Probes™, A22066). Mitochondria were stirred in MRB at 0.5 mg/ml with 1 mg/ml fat-free BSA, 600 μM ADP, and 2 μM rotenone. 5 mM succinate was used for a control for maximum ATP level, and 0.001 mg/ml oligomycin A was used as a zero ATP synthesis control. Mitochondrial suspensions were immediately frozen with liquid nitrogen after 1, 5, or 10 min light exposure (XCite LED, 0.02 mW/mm^2). Samples were then thawed on ice, centrifuged at 14,800 *g*, and supernatant was collected and run at 1:100 dilution in MRB in the luminescence assay. Oligomycin A control values were subtracted from experimental reads, and data were then normalized to luminescent signal from succinate control samples (complete ADP conversion confirmed by monitoring O_2 consumption rate transitions).

Mitochondrial O_2 consumption

O_2 consumption was measured using a Clark-type O_2 electrode (S1 electrode disk, DW2/2 electrode chamber and Oxy-Lab control unit, Hansatech Instruments, Norfolk UK) at 25°C. Isolated mitochondria were stirred in MRB at 1 mg/ml with 1 mg/ml fat-free BSA. Substrates and inhibitors were added by syringe port (100 μM ADP, 2 μM rotenone, 5 mM succinate). Given excess succinate as substrate for ETC respiration, we measured the amount of O_2 required to convert 50 nmol of ADP to ATP and established a baseline for comparison. To test mtON activity, we illuminated mitochondria as in the ATP measurement, for 1, 5, or 10 min in the presence of ADP without succinate to allow for mtON conversion of ADP to ATP. Any remaining ADP was then converted using O_2-dependent ETC respiration upon succinate addition (Fig EV4C). Slopes were calculated from plots of O_2 concentration versus time to give rates of O_2 consumption during ADP respiration, ADP+succinate respiration, and respiration after ADP had been entirely consumed. The intersections of these three rates were used to calculate total amount of O_2 consumed during ADP+succinate respiration. Light activation of mitochondria (XCite LED, 0.02 mW/mm^2) during ADP respiration alone was carried out for differing lengths of time to test the ability of mtON to drive ADP consumption before succinate was added. Dark control was 10 min of no illumination before addition of succinate.

ETC inhibitor assays

Experiments were performed on at least three separate days, using 15–100 young adult animals per plate. Seeded plates were supplemented with rotenone (50 μM final concentration), antimycin A (50 μM final concentration), or oligomycin A (31 μM final concentration) 24 h before animals were transferred onto them. For azide toxicity, animals were placed in M9 buffer with 250 mM azide. Control plates were kept in the dark, and experimental plates were exposed to 1 Hz light (Quantum LED, 0.02 mW/mm^2) for the duration of the experiment. For all toxins, animals that were moving or those that moved in response to a light touch to the head were scored as alive. For rotenone, surviving animals were scored after 5 h. For antimycin A, animals were scored 16 h after exposure. For azide, animals were exposed for 1 h in M9 and allowed to recover for 1 h on a seeded culture plate and then survival was scored. Azide experimental plates were exposed to light (XCite LED, 0.19 mW/mm^2) for the duration of azide treatment and recovery. For oligomycin, animals were scored 18 h after exposure. For oligomycin A, animals were scored 18 h after exposure.

Locomotion assay

Locomotion was scored by counting the number of body bends in 15 s immediately after being transferred off OP50 food [85] (n = 36–46 animals scored on at least 2 separate days). One body bend was scored as a deflection of direction of motion of the posterior pharyngeal bulb [86]. For AMPK activation, animals were placed on plates containing 1 mM AICAR 4 h before counting body bends. AICAR was dissolved in M9 buffer, added directly onto OP50 seeded plates, and allowed to dry. Illumination was continuous through measurements (MVX, 0.265 mW/mm^2).

Mitochondrial DNA PCR

The uaDf5 mitochondrial DNA deletion [49] was detected by PCR amplification as described [87] from whole-animal lysate. Briefly, using primers for wild-type mitochondrial DNA (forward: TTGGTGTTACAGGGGCAACA, reverse: CTTCTACAGTGCATTGAC CTAGTC, expected size: ~500 bp) and for uaDf5 DNA (forward: CCATCCGTGCTAGAAGACAA, reverse: CTTCTACAGTGCATTGACC TAGTC, expected size ~299 bp), PCR was performed as follows: 98°C for 30 s for melting, 55°C for 30 s for annealing, and 72°C for 30 s for elongation, for 35 cycles. Mitochondrial DNA was visualized by electrophoresis through 2% agarose gel stained with ethidium bromide.

uaDf5 progeny survival

Single L4 animals were placed on seeded plates and allowed to develop through egg laying. The number of progeny was scored after 4 days, where light treatment was throughout (Quantum LED, 0.02 mW/mm^2) for the duration of the experiment for +light conditions. Progeny were scored as the number of animals that developed to L4 stage.

Hypoxia and reoxygenation

Experiments were carried out using a hypoxic chamber (Coy Laboratory Products, 5%/95% H_2/N_2 gas, palladium catalyst) at 26°C with 50–100 animals per plate. O_2 was < 0.01%. Hypoxic preconditioning (PC) duration was 4 h, and control animals were incubated at 26°C in room air for the same time. 1 Hz illumination (Quantum LED, 0.02 mW/mm^2) was carried out during PC period or during the hypoxic period. Hypoxic exposure was for 18.5, 21 h after PC. Twenty-four hours after hypoxia exposure, animals that were moving or those that moved in response to a light touch to the head were scored as alive. Data from days where PC was at least 15% effective for both +ATR and −ATR were used. Animals supplemented with ATR were allowed to lay eggs onto plates with no ATR that were subsequently used for HR experiments to minimize confounding effects of ATR. ATR from the parent animal was sufficient to provide active mtON in progeny as tested by the azide toxin assay described above. Only progeny from parents supplemented with ATR were significantly protected against azide upon illumination (tested by one-way ANOVA, −ATR, −light [17.3% survival] versus +ATR, +light [66.8% survival] $P = 0.0054$, −ATR, +light [32.5% survival] versus +ATR, +light $P = 0.0395$, +ATR, −light [27.5% survival] versus +ATR, +light $P = 0.0199$, DF = 11, $F = 8.94$). PC experiments were represented as protection (%), where baseline survival was subtracted to correct for protection from ATR (−ATR survival: 34.4 ± 14.4%, +ATR survival: 49.7 ± 20.3%, 2-sample 2-tailed paired t-test, $P = 0.033$, n = 12 independent experiments). FCCP dissolved in ethanol was deposited onto seeded NGM plates to the final concentrations indicated in the figure legend (Fig 5C).

Statistics

One-way ANOVA was used when comparing only our four experimental conditions (Fig EV2). Two-way ANOVA was used when comparing our conditions with other variables, such as +/− succinate. Shapiro–Wilk normality tests were used to determine whether parametric or non-parametric tests should be used. See figure legends for detailed statistical information and post hoc tests.

Data availability

All data are presented in the manuscript, and raw files will be made available upon request.

Expanded View for this article is available online.

Acknowledgements

Work in the laboratory of A.P.W. is supported by a grant from National Institutes of Health (R01 NS092558) and institutional funds from the University of Rochester; B.J.B. is supported by an American Heart Association Predoctoral Fellowship (18PRE33990054) and an Institutional Ruth L. Kirschstein National Research Service Award (NIH T32 GM068411). Y.L. is supported by NSF IOS1753742. A.J.T current address: Institute for Physical Activity and Nutrition (IPAN), Deakin University, Burwood, Australia. We thank the members of the mitochondrial research groups at University of Rochester Medical Center for helpful discussions, suggestions, and guidance. Some strains were provided by the CGC, which is funded by NIH Office of Research Infrastructure Programs (P40 OD010440).

Author contributions

BJB and APW designed the research. BJB, AJT, ASM, AB, AMA, and YL performed experiments. MK provided critical review of the results and manuscript. BJB analyzed the data and wrote the manuscript. All authors approved the final version of the manuscript.

Conflict of interest

The authors declare that they have no conflict of interest.

References

1. Shadel GS, Horvath TL (2015) Mitochondrial ROS signaling in organismal homeostasis. *Cell* 163: 560 – 569
2. Rizzuto R, De Stefani D, Raffaello A, Mammucari C (2012) Mitochondria as sensors and regulators of calcium signalling. *Nat Rev Mol Cell Biol* 13: 566 – 578
3. Garrido C, Galluzzi L, Brunet M, Puig PE, Didelot C, Kroemer G (2006) Mechanisms of cytochrome c release from mitochondria. *Cell Death Differ* 13: 1423 – 1433
4. Dingley S, Polyak E, Lightfoot R, Ostrovsky J, Rao M, Greco T, Ischiropoulos H, Falk MJ (2010) Mitochondrial respiratory chain dysfunction variably increases oxidant stress in *Caenorhabditis elegans*. *Mitochondrion* 10: 125 – 136
5. Berry BJ, Trewin AJ, Amitrano AM, Kim M, Wojtovich AP (2018) Use the protonmotive force: mitochondrial uncoupling and reactive oxygen species. *J Mol Biol* 430: 3873 – 3891
6. Chalmers S, Saunter CD, Girkin JM, McCarron JG (2015) Flicker-assisted localization microscopy reveals altered mitochondrial architecture in hypertension. *Sci Rep* 5: 16875
7. Santo-Domingo J, Giacomello M, Poburko D, Scorrano L, Demaurex N (2013) OPA1 promotes pH flashes that spread between contiguous mitochondria without matrix protein exchange. *EMBO J* 32: 1927 – 1940
8. Glancy B, Hartnell LM, Combs CA, Femnou A, Sun J, Murphy E, Subramaniam S, Balaban RS (2018) Power grid protection of the muscle mitochondrial reticulum. *Cell Rep* 23: 2832
9. Chalmers S, Caldwell ST, Quin C, Prime TA, James AM, Cairns AG, Murphy MP, McCarron JG, Hartley RC (2012) Selective uncoupling of individual mitochondria within a cell using a mitochondria-targeted photoactivated protonophore. *J Am Chem Soc* 134: 758 – 761
10. Zhang L, Trushin S, Christensen TA, Bachmeier BV, Gateno B, Schroeder A, Yao J, Itoh K, Sesaki H, Poon WW *et al* (2016) Altered brain energetics induces mitochondrial fission arrest in Alzheimer's disease. *Sci Rep* 6: 18725
11. Solaini G, Baracca A, Lenaz G, Sgarbi G (2010) Hypoxia and mitochondrial oxidative metabolism. *Biochim Biophys Acta* 1797: 1171 – 1177
12. Murphy MP, Hartley RC (2018) Mitochondria as a therapeutic target for common pathologies. *Nat Rev Drug Discov* 17: 865 – 886
13. Yang JL, Mukda S, Chen SD (2018) Diverse roles of mitochondria in ischemic stroke. *Redox Biol* 16: 263 – 275
14. Tkatch T, Greotti E, Baranauskas G, Pendin D, Roy S, Nita LI, Wettmarshausen J, Prigge M, Yizhar O, Shirihai OS *et al* (2017) Optogenetic control of mitochondrial metabolism and Ca(2 +) signaling by mitochondria-targeted opsins. *Proc Natl Acad Sci USA* 114: E5167 – E5176
15. Ernst P, Xu N, Qu J, Chen H, Goldberg MS, Darley-Usmar V, Zhang JJ, O'Rourke B, Liu X, Zhou L (2019) Precisely control mitochondria with light to manipulate cell fate decision. *Biophys J* 117: 631 – 645
16. Chow BY, Han X, Dobry AS, Qian X, Chuong AS, Li M, Henninger MA, Belfort GM, Lin Y, Monahan PE *et al* (2010) High-performance genetically targetable optical neural silencing by light-driven proton pumps. *Nature* 463: 98 – 102
17. Husson SJ, Liewald JF, Schultheis C, Stirman JN, Lu H, Gottschalk A (2012) Microbial light-activatable proton pumps as neuronal inhibitors to functionally dissect neuronal networks in *Caenorhabditis elegans*. *PLoS ONE* 7: e40937
18. Kandori H (2015) Ion-pumping microbial rhodopsins. *Front Mol Biosci* 2: 52
19. Trewin AJ, Berry BJ, Wei AY, Bahr LL, Foster TH, Wojtovich AP (2018) Light-induced oxidant production by fluorescent proteins. *Free Radic Biol Med* 128: 157 – 164
20. Rost BR, Schneider F, Grauel MK, Wozny C, Bentz C, Blessing A, Rosenmund T, Jentsch TJ, Schmitz D, Hegemann P *et al* (2015) Optogenetic acidification of synaptic vesicles and lysosomes. *Nat Neurosci* 18: 1845 – 1852
21. Ernst P, Xu N, Song J, Qu J, Chen H, Goldberg MS, Zhang J, O'Rourke B, Liu X, Zhou L (2018) Precisely control mitochondrial membrane potential with light to manipulate cell fate decisions. *bioRxiv* https://doi.org/10.1101/469668469668 [PREPRINT]
22. Trewin AJ, Bahr LL, Almast A, Berry BJ, Wei AY, Foster TH, Wojtovich AP (2019) Mitochondrial reactive oxygen species generated at the complex-II matrix or intermembrane space microdomain have distinct effects on redox signaling and stress sensitivity in *Caenorhabditis elegans*. *Antioxid Redox Signal* 31: 594 – 607
23. Hara KY, Wada T, Kino K, Asahi T, Sawamura N (2013) Construction of photoenergetic mitochondria in cultured mammalian cells. *Sci Rep* 3: 1635
24. Waschuk SA, Bezerra AG Jr, Shi L, Brown LS (2005) Leptosphaeria rhodopsin: bacteriorhodopsin-like proton pump from a eukaryote. *Proc Natl Acad Sci USA* 102: 6879 – 6883
25. Tsang WY, Lemire BD (2003) The role of mitochondria in the life of the nematode, *Caenorhabditis elegans*. *Biochim Biophys Acta* 1638: 91 – 105
26. Butler JA, Ventura N, Johnson TE, Rea SL (2010) Long-lived mitochondrial (Mit) mutants of *Caenorhabditis elegans* utilize a novel metabolism. *FASEB J* 24: 4977 – 4988
27. Wang YT, Lim Y, McCall MN, Huang KT, Haynes CM, Nehrke K, Brookes PS (2019) Cardioprotection by the mitochondrial unfolded protein response (UPR(mt)) requires ATF5. *Am J Physiol Heart Circ Physiol* 317: H472 – H478
28. Pena S, Sherman T, Brookes PS, Nehrke K (2016) The mitochondrial unfolded protein response protects against anoxia in *Caenorhabditis elegans*. *PLoS ONE* 11: e0159989
29. Wojtovich AP, Nadtochiy SM, Urciuoli WR, Smith CO, Grunnet M, Nehrke K, Brookes PS (2013) A non-cardiomyocyte autonomous mechanism of cardioprotection involving the SLO1 BK channel. *PeerJ* 1: e48
30. Wojtovich AP, Nadtochiy SM, Brookes PS, Nehrke K (2012) Ischemic preconditioning: the role of mitochondria and aging. *Exp Gerontol* 47: 1 – 7
31. John GB, Shang Y, Li L, Renken C, Mannella CA, Selker JM, Rangell L, Bennett MJ, Zha J (2005) The mitochondrial inner membrane protein mitofilin controls cristae morphology. *Mol Biol Cell* 16: 1543 – 1554
32. Fischer LR, Igoudjil A, Magrane J, Li Y, Hansen JM, Manfredi G, Glass JD (2011) SOD1 targeted to the mitochondrial intermembrane space prevents motor neuropathy in the Sod1 knockout mouse. *Brain* 134: 196 – 209

33. Sumii M, Furutani Y, Waschuk SA, Brown LS, Kandori H (2005) Strongly hydrogen-bonded water molecule present near the retinal chromophore of *Leptosphaeria rhodopsin*, the bacteriorhodopsin-like proton pump from a eukaryote. *Biochemistry* 44: 15159 – 15166
34. Okazaki A, Takagi S (2013) An optogenetic application of proton pump ArchT to *Caenorhabditis elegans* cells. *Neurosci Res* 75: 29 – 34
35. Takahashi M, Takagi S (2017) Optical silencing of body wall muscles induces pumping inhibition in *Caenorhabditis elegans*. *PLoS Genet* 13: e1007134
36. Porcelli AM, Ghelli A, Zanna C, Pinton P, Rizzuto R, Rugolo M (2005) pH difference across the outer mitochondrial membrane measured with a green fluorescent protein mutant. *Biochem Biophys Res Commun* 326: 799 – 804
37. Glancy B, Hartnell LM, Malide D, Yu ZX, Combs CA, Connelly PS, Subramaniam S, Balaban RS (2015) Mitochondrial reticulum for cellular energy distribution in muscle. *Nature* 523: 617 – 620
38. Balaban RS, Kantor HL, Katz LA, Briggs RW (1986) Relation between work and phosphate metabolite in the *in vivo* paced mammalian heart. *Science* 232: 1121 – 1123
39. Viola HM, Hool LC (2017) Auto-regulation in the powerhouse. *Elife* 6: e28757
40. Wang X, Zhang X, Wu D, Huang Z, Hou T, Jian C, Yu P, Lu F, Zhang R, Sun T *et al* (2017) Mitochondrial flashes regulate ATP homeostasis in the heart. *Elife* 6: e23908
41. Brand MD, Nicholls DG (2011) Assessing mitochondrial dysfunction in cells. *Biochem J* 435: 297 – 312
42. Ishiguro H, Yasuda K, Ishii N, Ihara K, Ohkubo T, Hiyoshi M, Ono K, Senoo-Matsuda N, Shinohara O, Yosshii F *et al* (2001) Enhancement of oxidative damage to cultured cells and *Caenorhabditis elegans* by mitochondrial electron transport inhibitors. *IUBMB Life* 51: 263 – 268
43. Schmeisser S, Priebe S, Groth M, Monajembashi S, Hemmerich P, Guthke R, Platzer M, Ristow M (2013) Neuronal ROS signaling rather than AMPK/sirtuin-mediated energy sensing links dietary restriction to lifespan extension. *Mol Metab* 2: 92 – 102
44. Siddikuzzaman Grace VM (2013) Antioxidant potential of all-trans retinoic acid (ATRA) and enhanced activity of liposome encapsulated ATRA against inflammation and tumor-directed angiogenesis. *Immunopharmacol Immunotoxicol* 35: 164 – 173
45. Lee HP, Casadesus G, Zhu X, Lee HG, Perry G, Smith MA, Gustaw-Rothenberg K, Lerner A (2009) All-trans retinoic acid as a novel therapeutic strategy for Alzheimer's disease. *Expert Rev Neurother* 9: 1615 – 1621
46. Palace VP, Khaper N, Qin Q, Singal PK (1999) Antioxidant potentials of vitamin A and carotenoids and their relevance to heart disease. *Free Radic Biol Med* 26: 746 – 761
47. Morgan PG, Sedensky MM (1994) Mutations conferring new patterns of sensitivity to volatile anesthetics in *Caenorhabditis elegans*. *Anesthesiology* 81: 888 – 898
48. Melo JA, Ruvkun G (2012) Inactivation of conserved *Caenorhabditis elegans* genes engages pathogen- and xenobiotic-associated defenses. *Cell* 149: 452 – 466
49. Tsang WY, Lemire BD (2002) Stable heteroplasmy but differential inheritance of a large mitochondrial DNA deletion in nematodes. *Biochem Cell Biol* 80: 645 – 654
50. Lin YF, Schulz AM, Pellegrino MW, Lu Y, Shaham S, Haynes CM (2016) Maintenance and propagation of a deleterious mitochondrial genome by the mitochondrial unfolded protein response. *Nature* 533: 416 – 419
51. Rea SL (2005) Metabolism in the *Caenorhabditis elegans* Mit mutants. *Exp Gerontol* 40: 841 – 849
52. Rea SL, Ventura N, Johnson TE (2007) Relationship between mitochondrial electron transport chain dysfunction, development, and life extension in *Caenorhabditis elegans*. *PLoS Biol* 5: e259
53. Rolland SG, Schneid S, Schwarz M, Rackles E, Fischer C, Haeussler S, Regmi SG, Yeroslaviz A, Habermann B, Mokranjac D *et al* (2019) Compromised mitochondrial protein import acts as a signal for UPR(mt). *Cell Rep* 28: 1659 – 1669 e1655
54. Imai Y, Inoshita T, Meng H, Shiba-Fukushima K, Hara KY, Sawamura N, Hattori N (2019) Light-driven activation of mitochondrial proton-motive force improves motor behaviors in a *Drosophila* model of Parkinson's disease. *Commun Biol* 2: 424
55. Hardie DG, Ross FA, Hawley SA (2012) AMPK: a nutrient and energy sensor that maintains energy homeostasis. *Nat Rev Mol Cell Biol* 13: 251 – 262
56. Apfeld J, O'Connor G, McDonagh T, DiStefano PS, Curtis R (2004) The AMP-activated protein kinase AAK-2 links energy levels and insulin-like signals to lifespan in *Caenorhabditis elegans*. *Genes Dev* 18: 3004 – 3009
57. Cunningham KA, Bouagnon AD, Barros AG, Lin L, Malard L, Romano-Silva MA, Ashrafi K (2014) Loss of a neural AMP-activated kinase mimics the effects of elevated serotonin on fat, movement, and hormonal secretions. *PLoS Genet* 10: e1004394
58. Lee H, Cho JS, Lambacher N, Lee J, Lee SJ, Lee TH, Gartner A, Koo HS (2008) The *Caenorhabditis elegans* AMP-activated protein kinase AAK-2 is phosphorylated by LKB1 and is required for resistance to oxidative stress and for normal motility and foraging behavior. *J Biol Chem* 283: 14988 – 14993
59. Garcia D, Shaw RJ (2017) AMPK: mechanisms of cellular energy sensing and restoration of metabolic balance. *Mol Cell* 66: 789 – 800
60. Hardie DG (2011) AMP-activated protein kinase: an energy sensor that regulates all aspects of cell function. *Genes Dev* 25: 1895 – 1908
61. Trewin AJ, Berry BJ, Wojtovich AP (2018) Exercise and mitochondrial dynamics: keeping in shape with ROS and AMPK. *Antioxidants* 7: E7
62. Hinchy EC, Gruszczyk AV, Willows R, Navaratnam N, Hall AR, Bates G, Bright TP, Krieg T, Carling D, Murphy MP (2018) Mitochondria-derived ROS activate AMP-activated protein kinase (AMPK) indirectly. *J Biol Chem* 293: 17208 – 17217
63. Mihaylova MM, Shaw RJ (2011) The AMPK signalling pathway coordinates cell growth, autophagy and metabolism. *Nat Cell Biol* 13: 1016 – 1023
64. Jeon SM (2016) Regulation and function of AMPK in physiology and diseases. *Exp Mol Med* 48: e245
65. Sanderson TH, Reynolds CA, Kumar R, Przyklenk K, Huttemann M (2013) Molecular mechanisms of ischemia-reperfusion injury in brain: pivotal role of the mitochondrial membrane potential in reactive oxygen species generation. *Mol Neurobiol* 47: 9 – 23
66. Chouchani ET, Pell VR, Gaude E, Aksentijevic D, Sundier SY, Robb EL, Logan A, Nadtochiy SM, Ord ENJ, Smith AC *et al* (2014) Ischaemic accumulation of succinate controls reperfusion injury through mitochondrial ROS. *Nature* 515: 431 – 435
67. Xu M, Wang Y, Ayub A, Ashraf M (2001) Mitochondrial K(ATP) channel activation reduces anoxic injury by restoring mitochondrial membrane potential. *Am J Physiol Heart Circ Physiol* 281: H1295 – H1303
68. Michiels C (2004) Physiological and pathological responses to hypoxia. *Am J Pathol* 164: 1875 – 1882
69. Dasgupta N, Patel AM, Scott BA, Crowder CM (2007) Hypoxic preconditioning requires the apoptosis protein CED-4 in *Caenorhabditis elegans*. *Curr Biol* 17: 1954 – 1959

70. Wojtovich AP, DiStefano P, Sherman T, Brookes PS, Nehrke K (2012) Mitochondrial ATP-sensitive potassium channel activity and hypoxic preconditioning are independent of an inwardly rectifying potassium channel subunit in *Caenorhabditis elegans*. *FEBS Lett* 586: 428 – 434
71. Jia B, Crowder CM (2008) Volatile anesthetic preconditioning present in the invertebrate *Caenorhabditis elegans*. *Anesthesiology* 108: 426 – 433
72. Hayakawa T, Kato K, Hayakawa R, Hisamoto N, Matsumoto K, Takeda K, Ichijo H (2011) Regulation of anoxic death in *Caenorhabditis elegans* by mammalian apoptosis signal-regulating kinase (ASK) family proteins. *Genetics* 187: 785 – 792
73. Ozcan C, Palmeri M, Horvath TL, Russell KS, Russell RR III (2013) Role of uncoupling protein 3 in ischemia-reperfusion injury, arrhythmias, and preconditioning. *Am J Physiol Heart Circ Physiol* 304: H1192 – H1200
74. Brennan JP, Southworth R, Medina RA, Davidson SM, Duchen MR, Shattock MJ (2006) Mitochondrial uncoupling, with low concentration FCCP, induces ROS-dependent cardioprotection independent of KATP channel activation. *Cardiovasc Res* 72: 313 – 321
75. Brennan JP, Berry RG, Baghai M, Duchen MR, Shattock MJ (2006) FCCP is cardioprotective at concentrations that cause mitochondrial oxidation without detectable depolarisation. *Cardiovasc Res* 72: 322 – 330
76. Shabalina IG, Nedergaard J (2011) Mitochondrial ("mild") uncoupling and ROS production: physiologically relevant or not? *Biochem Soc Trans* 39: 1305 – 1309
77. De Magalhaes Filho CD, Henriquez B, Seah NE, Evans RM, Lapierre LR, Dillin A (2018) Visible light reduces *Caenorhabditis elegans* longevity. *Nat Commun* 9: 927
78. Padilla PA, Ladage ML (2012) Suspended animation, diapause and quiescence: arresting the cell cycle in *Caenorhabditis elegans*. *Cell Cycle* 11: 1672 – 1679
79. Ghose P, Park EC, Tabakin A, Salazar-Vasquez N, Rongo C (2013) Anoxia-reoxygenation regulates mitochondrial dynamics through the hypoxia response pathway, SKN-1/Nrf, and stomatin-like protein STL-1/SLP-2. *PLoS Genet* 9: e1004063
80. Mello CC, Kramer JM, Stinchcomb D, Ambros V (1991) Efficient gene transfer in *Caenorhabditis elegans*: extrachromosomal maintenance and integration of transforming sequences. *EMBO J* 10: 3959 – 3970
81. Paix A, Folkmann A, Seydoux G (2017) Precision genome editing using CRISPR-Cas9 and linear repair templates in *Caenorhabditis elegans*. *Methods* 121–122: 86 – 93
82. Philip NS, Escobedo F, Bahr LL, Berry BJ, Wojtovich AP (2019) Mos1 element-mediated CRISPR integration of transgenes in *Caenorhabditis elegans*. *G3* 9: 2629 – 2635
83. Perry SW, Norman JP, Barbieri J, Brown EB, Gelbard HA (2011) Mitochondrial membrane potential probes and the proton gradient: a practical usage guide. *Biotechniques* 50: 98 – 115
84. Aldakkak M, Stowe DF, Cheng Q, Kwok WM, Camara AK (2010) Mitochondrial matrix K+ flux independent of large-conductance Ca2 + -activated K+ channel opening. *Am J Physiol Cell Physiol* 298: C530 – C541
85. Sawin ER, Ranganathan R, Horvitz HR (2000) *Caenorhabditis elegans* locomotory rate is modulated by the environment through a dopaminergic pathway and by experience through a serotonergic pathway. *Neuron* 26: 619 – 631
86. Tsalik EL, Hobert O (2003) Functional mapping of neurons that control locomotory behavior in *Caenorhabditis elegans*. *J Neurobiol* 56: 178 – 197
87. Lim Y, Rubio-Pena K, Sobraske PJ, Molina PA, Brookes PS, Galy V, Nehrke K (2019) Fndc-1 contributes to paternal mitochondria elimination in *Caenorhabditis elegans*. *Dev Biol* 454: 15 – 20

